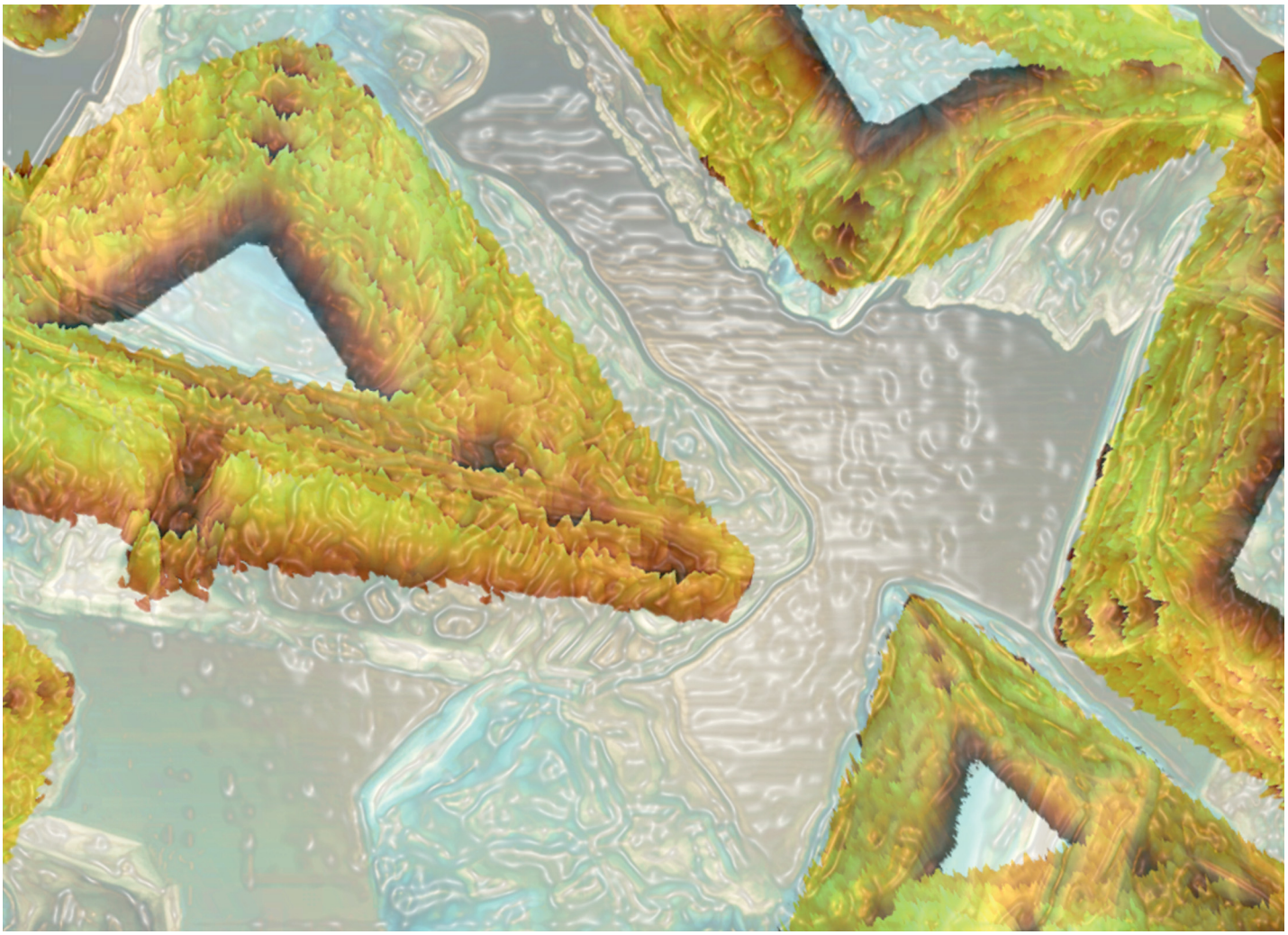

**Showcasing research from Professor Karim Fahmy's Biophysics Department at Helmholtz-Zentrum Dresden-Rossendorf, Institute for Resource Ecology and Technische Universität Dresden, Germany**

Cold denaturation of DNA origami nanostructures

Cold denaturation signifies the loss of native protein structure upon cooling under mildly denaturing conditions. This is shown to be also true for DNA origami. However, these larger structures amplify cold-induced strain into observable nanoscopic damage at predisposed sites.

## As featured in:


See Adrian Keller, Karim Fahmy *et al.*, *Chem. Commun.*, 2024, **60**, 5590.

ROYAL SOCIETY OF CHEMISTRY

rsc.li/chemcomm

Registered charity number: 207890

ChemComm

COMMUNICATION

View Article Online
View Journal | View Issue



Cite this: *Chem. Commun.*, 2024, **60**, 5590

Received 8th December 2023,
Accepted 9th April 2024

DOI: 10.1039/d3cc05985e

rsc.li/chemcomm



# Cold denaturation of DNA origami nanostructures†

Daniel Dornbusch,[ac] Marcel Hanke,[b] Emilia Tomm,[b] Charlotte Kielar,[ad] Guido Grundmeier,[b] Adrian Keller *[b] and Karim Fahmy *[ac]

**The coupling of structural transitions to heat capacity changes leads to destabilization of macromolecules at both elevated and lowered temperatures. DNA origami not only exhibit this property but also provide a nanoscopic observable of cold denaturation processes by directing intramolecular strain to the most sensitive elements within their hierarchical architecture.**

Cold denaturation, *i.e.*, the partial loss of structure in macromolecules upon a drop in temperature, is a well-known phenomenon observed for many proteins. It results from a positive change in heat capacity $\Delta c_p$ upon protein unfolding, whereby the denatured state becomes enthalpically favored at lower temperature.[1,2] Here, the aqueous exposure of hydrophobic molecular surfaces raises the heat capacity of interfacial water. As a consequence, native and partially unfolded states are equally populated at two temperatures $T_c$ (''cold'') and $T_w$ (''warm''). Few proteins undergo cold denaturation above 0 °C[3,4] but the majority do so in the presence of denaturants, *e.g.*, guanidinium chloride (GdmCl), which raises $T_c$ by structural destabilization.[1,5–7] For nucleic acids, reports of cold denaturation are conspicuously rare, but it has been observed for the hammerhead ribozyme in methanol-containing solutions at temperatures below 0 °C.[8,9]

In this communication, we demonstrate for the first time the cold denaturation of double-stranded (ds) DNA in GdmCl-containing solution at temperatures above 0 °C. Principle component analysis (PCA) of temperature-dependent circular dichroism (CD) spectra and thermodynamic modelling allowed determining $\Delta c_p$ which is causative for the cold denaturation of a DNA origami nanostructure.[10] DNA origami triangles amplify small conformational changes by their accumulation over the large number of linked dsDNA segments. Thereby, nanostructural changes are observable long before global heat denaturation in the presence of various concentrations of Gdm salts.[11] For 4 M GdmCl, *i.e.*, in the concentration range used for studying cold denaturation of proteins, DNA origami stability was maximal at 25 °C to 30 °C. Surprisingly, stability decreased not only by heating, but also by cooling, whereas DNA origami are not cold-sensitive in the absence of the denaturant.[12] The non-monotonic temperature dependence of stability led us to suggest that Gdm and its counter anions modulate $\Delta c_p$ which accompanies the thermally induced damage of DNA. In order to test this hypothesis, we explore here by CD spectroscopy the DNA origami nanostructure in the previously not covered temperature range between 20 °C and 1 °C performing closely spaced temperature sampling of the spectra. Thus, changes in the dsDNA upon altered base stacking interactions are detected. Fig. 1a shows the temperature-dependent CD spectra of DNA origami triangles in 4 M GdmCl. Stacking changes upon cooling from 35 °C to 1 °C are evident from the broadening and increase in CD amplitude at the main spectral features around 280 nm (positive) and at 245 nm (negative), respectively, as visualized in the contour plot in Fig. 1b. The ''derivative-like'' temperature sensitivity of the CD spectra is shown in Fig. 1c. It was calculated from the raw data by spectral correlation using a sliding window correlation analysis as described earlier.[11] The red colored region above 28 °C marks the decrease of the negative CD at 245 nm with the onset of heat denaturation. The blue colored region reflects the decrease of the positive CD amplitude upon cold denaturation. Between 15 °C and 30 °C, the spectral response to temperature is maximal throughout the entire wavelength range indicating cold-induced structural transitions. These were further evaluated by principal component analysis (PCA). Thus obtained spectral components cannot be correlated directly with physically distinct structures.

[a] *Helmholtz-Zentrum Dresden-Rossendorf, Institute of Resource Ecology, Bautzner Landstrasse 400, Dresden 01328, Germany. E-mail: k.fahmy@hzdr.de*
[b] *Paderborn University, Technical and Macromolecular Chemistry, Warburger Str. 100, Paderborn 33098, Germany. E-mail: adrian.keller@uni-paderborn.de*
[c] *Technische Universität Dresden, BIOTEC, Cluster of Excellence Physics of Life, Dresden 01062, Germany*
[d] *Helmholtz-Zentrum Dresden-Rossendorf, Institute for Ion Beam Physics and Materials Research, Bautzner Landstrasse 400, Dresden 01328, Germany*

† Electronic supplementary information (ESI) available: DNA origami synthesis; AFM imaging; CD spectroscopy and principal component analysis; additional AFM images at 5 °C, 10 °C and 20 °C. See DOI: https://doi.org/10.1039/d3cc05985e

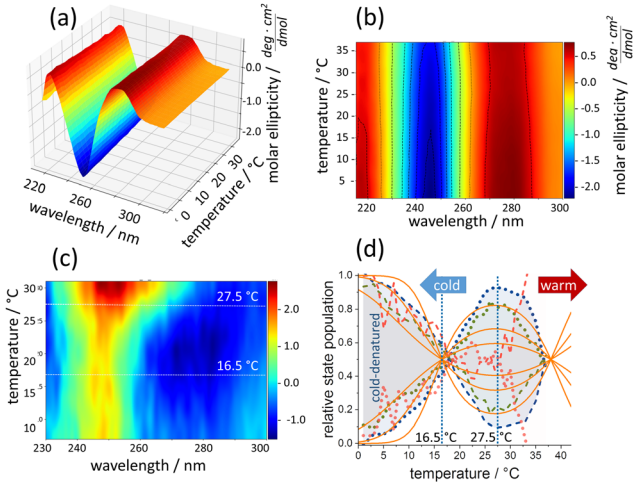


Fig. 1 (a) Temperature-dependent CD-spectra of DNA origami. (b) Contour plot of the same data. (c) Temperature sensitivity color-coded from low (blue) to high (red) sensitivity. (d) Temperature dependence of two principal CD-spectral components from the same experiments (dots and dashes). DNA structures between 16 °C and 28 °C (green and blue dots, two independent experiments) decrease upon cooling. The concomitant rise of the second component (dashes) falls in the temperature range of cold-induced DNA origami damage. A cold-warm-cold cycle renders DNA origami more temperature sensitive towards warming but preserves cold denaturation (red). Solid orange lines according to eqn (1) with (top to bottom) $\Delta H$/kJ: 220, 110, 55 and $\Delta c_p$/kJ K$^{-1}$: 2, 1, 0.5, respectively.

However, abstract components with maximal variance along the temperature axis have been determined, which resolve the general temperature sensitivity of chirality in the DNA origami as a whole. Approximating the CD spectra by only two structural populations leads to mirror-imaged curves of such abstract components as shown in Fig. 1d for three independent experiments. The first two experiments (green and blue traces) reveal the existence of a spectral phenotype that is maximally populated at ~27 °C in the ensemble of DNA origami nanostructures. Remarkably, this spectral phenotype becomes depopulated by both, heating and cooling of the sample, typical of structural transitions that are accompanied by a $\Delta c_p$. At 1 °C, its spectral weight vanishes. The underlying structural transitions do not follow the classical sigmoidal behavior of temperature-dependent equilibria because $\Delta c_p$ renders enthalpy and entropy themselves temperature-sensitive, instead of representing constant standard values. Whereas the shape of the obtained temperature sensitivity is an unambiguous result of the PCA, the location of the intersection between the two curves depends on additional information on the relative state populations. In a previous study, we showed that "intact" and "damaged" DNA origami in 4 M GdmCl are equally present at ~37 °C.[11] Fixing a crossing point at this temperature, leads to a second intersection of the obtained PCA traces at ~16 °C, where "intact" and "damaged" states are again equally frequent (inclusion of a third component altered this result only marginally, Fig. S1, ESI†). Thus, a spectral phenotype of "intact" triangles dominates between 16 °C and 37 °C, whereas it becomes depopulated above 37 °C and by cooling below 16 °C. The shaded areas in Fig. 3d visualize the population difference between the two spectral phenotypes for the two experiments. In a third experiment (red traces in Fig. 3d), the sample was cooled down from 37 °C to 1 °C, re-heated to 37 °C and again cooled down. In the second cooling process, the cold denaturation was still visible, demonstrating that it is a largely reversible process. However, the onset of heat denaturation in this sample became lowered to 25 °C, indicative of a structural destabilization during repeated temperature scans.

A structural interpretation of the CD-spectral change itself based on dsDNA model sequences would be highly speculative. However, the data do allow estimating the thermodynamic parameters of cold- and heat-inducible damage. We have simulated the thermal equilibrium between two states with temperature-dependent enthalpic and entropic terms to express the Gibbs free energy change of the structural transition as:

$$\Delta G_0(T) = \Delta H_0 \cdot (-\Delta T/T_m) + \Delta c_p \cdot [\Delta T - T \cdot \ln(T/T_m)] \quad (1)$$

This equation takes into account a $\Delta c_p$ upon structural transitions of the DNA origami from "intact" to cold-induced "damaged" in addition to a standard enthalpy change of $\Delta H_0$ (defined here for a temperature of $T_w$ = 38 °C, where "intact" and "damaged" triangles are equally populated). The solid lines in Fig. 3d show the two populations predicted for equilibrium states according to eqn (1). The curves were obtained with the $\Delta H_0$ and $\Delta c_p$ values given in the legend to Fig. 3d. The maximum and minimum state populations depend on the absolute value of $\Delta H_0$. However, the crossing points of equally populated states are unaffected as long as $\Delta c_p$ stays in constant proportion to $\Delta H_0$. The experimental results were best reproduced with the ratio $\Delta c_p/\Delta H_0$ of 0.09 which results in "cold" ($T_c$) and "warm" ($T_w$) denaturation temperatures of 16.5 °C and 38.0 °C, respectively. The data show that similar to proteins under denaturing conditions,[13,14] also DNA origami exhibit cold denaturation in the presence of GdmCl. Cold-denatured structures, however, need not correspond to their heat-denatured unfolded states. Cold-denatured proteins appear to be rather compact but water-invaded states.[15]

Having shown the nanoscopic response of DNA origami triangles to the accumulation of small base stacking changes long before heat denaturation, we looked for possible nanostructural changes that may accompany cold denaturation. Fig. 2 compares representative AFM images of DNA origami triangles between 20 °C and 5 °C, in which intact triangles coexist with partially damaged structures exhibiting dissociated vertices or collapsed shapes. The images were analyzed in detail by determining the occurrence of specific damages, such as dissociated vertices (dv), collapsed triangles (ct), and broken trapezoids (bt). The statistical analysis shows that the cold-induced increase of damaged DNA origami triangles (Fig. 3a) is predominantly caused by a growing number of dissociated vertices (Fig. 3b and c). Their population is doubled at 5 °C *versus* 20 °C, whereas other damage types are mostly unaffected. These data indicate that the denaturant may preferentially destabilize the vertices. On the other hand, the ct and bt damage types together make up 30–40% of the total number of triangles in line with the general destabilizing effect of GdmCl on the trapezoids as well.[11] It is the

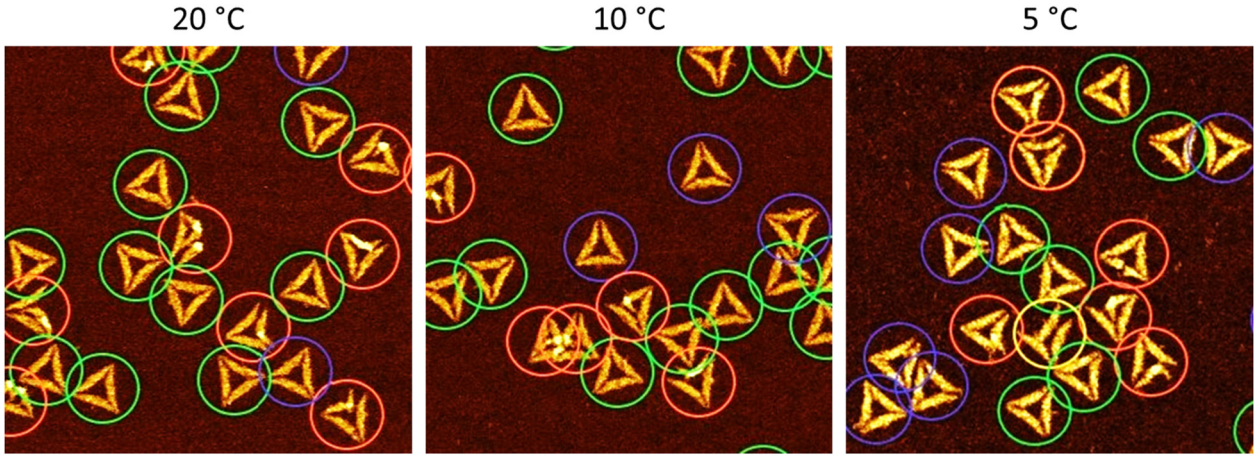


Fig. 2 AFM images (1 × 1 μm$^2$) of DNA origami triangles after incubation at 20 °C, 10 °C, and 5 °C, respectively. The colored circles indicate intact (green) and damaged triangles according to Fig. 3c (dv, violet; ct, yellow; bt, red). Height scales are 3.2 nm.

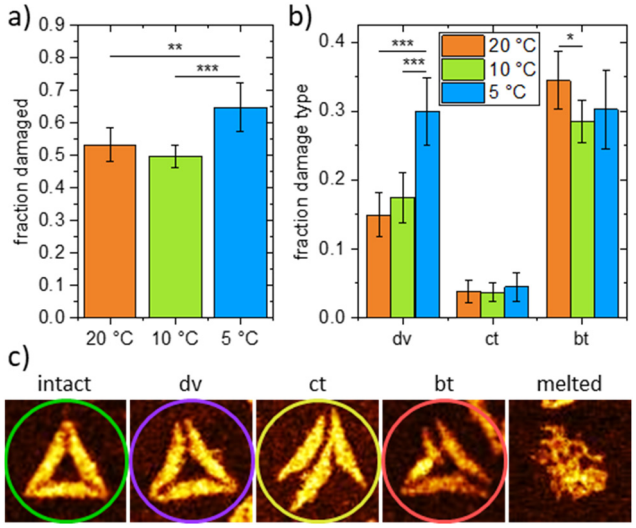


Fig. 3 (a) Total fraction of damaged DNA origami triangles after incubation at 20 °C, 10 °C, and 5 °C taken from 890, 949 and 844 DNA origami, respectively. (b) Fractions of different damage types (dv – dissociated vertices, ct – collapsed triangles, bt – broken trapezoids) observed after incubation at 20 °C, 10 °C, and 5 °C. (c) AFM images (0.179 × 0.179 μm$^2$) showing examples of intact and damaged DNA origami triangles. Height scales are 2.5 to 2.7 nm (intact, dv, ct, bt) and 3.7 nm (melted), respectively. Note that the melted DNA origami was obtained for an incubation temperature of 37 °C. This type of damage is not observed at lower temperatures. Statistical significances (two-tailed distribution, homoscedastic) are indicated as * ($p < 0.05$), ** ($p < 0.01$), and *** ($p < 0.001$).

sensitivity to cold denaturation, not to GdmCl *per se*, which distinguishes the vertices from the trapezoids. This suggests that cold-induced structural changes at the trapezoids lead to the accumulation of strain, which is then directed to the vertices, thereby, reducing further cold-induced damage in the trapezoids (beyond the basal damage induced by GdmCl itself). This agrees with the occurrence of triangles with dissociated vertices but mostly intact trapezoids, whereas triangles with broken trapezoids almost always show dissociated vertices.

Cold denaturation of proteins is well-known and has been thermodynamically analyzed in seminal studies particularly by the Privalov group[1] and is typically monitored by CD or NMR spectroscopy.[4,13,16,17] However, only few proteins exhibit cold denaturation at ambient temperatures.[4] Denaturants such as urea or GdmCl rise $T_c$ and have been used in protein cold-induced unfolding.[18–20] For DNA origami, cold-denaturation under these conditions has not yet been investigated at all. Our study shows that it is spectroscopically detectable as a global change in chirality, which is accompanied by rather local nanoscopic structural transitions. The "visibility" of cold-induced damage at specific sites of the supramolecular assembly is remarkable and not paralleled in scale by cold-denatured proteins. It indicates that temperature-dependent structural strain in the entire DNA assembly appears to be unevenly partitioned. Strain in base pairing and stacking is likely to accumulate along the repetitive structural elements of the DNA origami architecture and eventually concentrates at predisposed structural hotspots (whereas heat denaturation unfolds the entire structure[11]). Here, the accumulated cold-induced forces exceed local molecular interaction forces. CD spectroscopy picks up the global stacking changes at a molecular level, enabling the quantification of $\Delta c_p$ underlying cold denaturation. AFM imaging visualizes the nanoscopic consequences at particularly susceptible sites to the degree they can be resolved, whereas CD spectroscopy responds to the entirety of structural changes thus enabling thermodynamic modelling.

The non-monotonic temperature dependence of DNA origami damages modelled in Fig. 1d originates in a positive $\Delta c_p$ during the "intact" to "damaged" transition. In fact, DNA melting involves a positive $\Delta c_p$ between 134 and 420 J K$^{-1}$ mol-bp$^{-1}$ and scales with the increased of solvent-accessible apolar surface.[21] Typically, $\Delta c_p$ is by 2–4 larger than $\Delta S_0$ (105 J K$^{-1}$ mol-bp$^{-1}$).[22] At the reference temperature of 38 °C and the three examples of cold denaturation curves in Fig. 3d, the $\Delta S_0$ of the DNA origami transition (obtained as $\Delta S_0 = \Delta H_0/(311\ \mathrm{K})$) equals 708, 354 and 177 J K$^{-1}$, respectively. The corresponding $\Delta c_p$ values given in the

 

caption of Fig. 3d are indeed within the reported proportion. This suggests that GdmCl increased the $T_c$ above 0 °C, as it does for cold denaturation of proteins, without affecting the fundamental relation between $\Delta S_0$ and $\Delta c_p$ of dsDNA melting. Above 40 °C, the denaturant and its counterions are involved in more complex processes during melting of DNA origami.[11,23] The $\Delta H$ of base pair melting is about 19 kJ mol$^{-1}$ at 25 °C.[21] The simulation of cold-induced DNA origami damage with a $\Delta H_0$ of 200–300 kJ results in an acceptable approximation of our PCA data, suggesting that 10–15 base pairs break cooperatively. The number of such cooperative units cannot be deduced, but their estimated number of base pairs is comparable to the lengths of the bridging staples at the vertices (11 base pairs).[24] The consistency of spectroscopically inferred thermodynamic data and nanostructural damage suggests that the vertices are the predominant source of cold-induced exposure of hydrophobic surface of both, DNA bases and released $Gdm^+$ ions. Thus, dsDNA melting at the structurally most dynamic vertices[25] probably contributes to the global $\Delta c_p$ derived from CD spectroscopy. Adsorption of the originally twisted DNA origami[25,26] on mica induces strain in the entire nanostructure. The cold-induced concave appearance of the trapezoids seen in some dv states, is likely to be the consequence of released in-plane strain once the vertices no longer connect the individual trapezoids. In fact, damage at the vertices decreased and cold-denaturation was absent when global strain was released by disrupting the linkage between the two half sides in one of the three trapezoids (see ESI†).

In summary, our data show that DNA origami exhibit cold denaturation above 0 °C in the presence of GdmCl, similar to proteins. In contrast to the latter, DNA origami triangles show a response at the nm scale as cold-induced strain affects predisposed architectural motifs to rupture, allowing more relaxation at other sites of the nanostructure. Future DNA origami design may either exploit or prevent such effects.

Conceptualization, D. D., M. H., A. K., and K. F.; formal analysis, D. D., M. H., E. T., A. K., C. K., and K. F.; funding acquisition, A. K. and K. F.; investigation, D. D., M. H., C. K. and E. T.; methodology, D. D., M. H., A. K., C. K., and K. F.; project administration, A. K. and K. F.; resources, G. G.; supervision, G. G., A. K., and K. F.; validation, D. D., M. H., and E. T.; visualization, D. D., E. T., A. K., C. K., and K. F.; writing – original draft, A. K. and K. F.; writing – review and editing, D. D., M. H., E. T., G. G., A. K., and K. F.

This work was supported by the Deutsche Forschungsgemeinschaft (DFG) under grant number 428230890.

## Conflicts of interest

There are no conflicts to declare.

## Notes and references

1 P. L. Privalov, *Biophys. J.*, 1990, **57**, A26.
2 N. V. Prabhu and K. A. Sharp, *Annu. Rev. Phys. Chem.*, 2005, **56**, 521–548.
3 R. Yan, P. DeLos Rios, A. Pastore and P. A. Temussi, *Commun. Chem.*, 2018, **1**, 13.
4 A. Pastore, S. R. Martin, A. Politou, K. C. Kondapalli, T. Stemmler and P. A. Temussi, *J. Am. Chem. Soc.*, 2007, **129**, 5374–5375.
5 B. Ibarra-Molero, G. I. Makhatadze and J. M. Sanchez-Ruiz, *Biochim. Biophys. Acta*, 1999, **1429**, 384–390.
6 Y. Guo, R. A. Kammerer and J. Engel, *Biophys. Chem.*, 2000, **85**, 179–186.
7 X. L. Tang and M. J. Pikal, *Pharm. Res.*, 2005, **22**, 1167–1175.
8 P. J. Mikulecky and A. L. Feig, *Nucleic Acids Res.*, 2004, **32**, 3967–3976.
9 P. J. Mikulecky and A. L. Feig, *J. Am. Chem. Soc.*, 2002, **124** 890–891.
10 P. W. K. Rothemund, *Nature*, 2006, **440**, 297–302.
11 M. Hanke, D. Dornbusch, C. Hadlich, A. Rossberg, N. Hansen, G. Grundmeier, S. Tsushima, A. Keller and K. Fahmy, *Comput. Struct. Biotechnol. J.*, 2022, **20**, 2611–2623.
12 Y. Xin, C. Kielar, S. Zhu, C. Sikeler, X. Xu, C. Moser, G. Grundmeier, T. Liedl, A. Heuer-Jungemann, D. M. Smith and A. Keller, *Small*, 2020, **16**, e1905959.
13 R. Kitahara, A. Okuno, M. Kato, Y. Taniguchi, S. Yokoyarnal and K. Akasaka, *Magn. Reson. Chem.*, 2006, **44**, S108–S113.
14 Y. V. Griko, P. L. Privalov, S. Y. Venyaminov and V. P. Kutyshenko, *J. Mol. Biol.*, 1988, **202**, 127–138.
15 M. Davidovic, C. Mattea, J. Qvist and B. Halle, *J. Am. Chem. Soc.*, 2009, **131**, 1025–1036.
16 S. T. Whitten, A. J. Kurtz, M. S. Pometun, A. J. Wand and V. J. Hilser, *Biochemistry*, 2006, **45**, 10163–10174.
17 W. D. Van Horn, A. K. Simorellis and P. F. Flynn, *J. Am. Chem. Soc.*, 2005, **127**, 13553–13560.
18 B. L. Chen, W. A. Baase and J. A. Schellman, *Biochemistry*, 1989, **28**, 691–699.
19 B. L. Chen and J. A. Schellman, *Biochemistry*, 1989, **28**, 685–691.
20 Y. V. Griko, P. L. Privalov, J. M. Sturtevant and S. Y. Venyaminov, *Proc. Natl. Acad. Sci. U. S. A.*, 1988, **85**, 3343–3347.
21 A. Dragan, P. Privalov and C. Crane-Robinson, *Eur. Biophys. J.*, 2019, **48**, 773–779.
22 I. Rouzina and V. A. Bloomfield, *Biophys. J.*, 1999, **77**, 3242–3251.
23 M. Hanke, N. Hansen, E. Tomm, G. Grundmeier and A. Keller, *Int. J. Mol. Sci.*, 2022, **23**, 8547.
24 S. Ramakrishnan, G. Krainer, G. Grundmeier, M. Schlierf and A. Keller, *Nanoscale*, 2016, **8**, 10398–10405.
25 A. Suma, A. Stopar, A. W. Nicholson, M. Castronovo and V. Carnevale, *Nucleic Acids Res.*, 2020, **48**, 4672–4680.
26 S. Ramakrishnan, B. X. Shen, M. A. Kostiainen, G. Grundmeier, A. Keller and V. Linko, *ChemBioChem*, 2019, **20**, 2818–2823.